Opt Rev (2016) 23:637–645
DOI 10.1007/s10043-016-0226-6

REGULAR PAPER

Lidar observations of wind over Xin Jiang, China: general characteristics and variation

Yan Han[1,2,3] · Dong-song Sun[1] · Ning-quan Weng[2] · Jian-guo Wang[3] · Xian-kang Dou[1] · Yan-hong Zhang[3] · Jun Guan[3] · Qingjian Miao[3] · Xin Chen[3]

Received: 4 January 2016 / Accepted: 18 May 2016 / Published online: 1 June 2016

Abstract The mobile Rayleigh Doppler lidar based on a Fabry–Perot etalon is developed for wind measurement. The structure and technical parameters of this lidar system are described in brief. The 1740 wind profiles from 8 to 40 km altitudes by the lidar in Xinjiang, China, were obtained in 2010 and 2011, and were used to analyze the characteristics and variations of wind. The results shown that the wind velocity is within a three-layer structure: westerly jet layer (9–14 km), quasi-zero velocity layer (18–22 km) and gale layer (22–40 km). In August and September, the wind direction is within a three-layer structure: zonal westerly wind layer (5–18 km) where wind direction is west, zonal wind reverse layer (18–22 km) where wind direction is unstable and easterly wind layer (22–40 km) where wind direction is east. In October, wind direction is west (8–40 km). Wind observations by lidar are a realistic offset to the rawins.

Keywords Double-edge technology · Direct detection · Doppler wind lidar · Wind measurements · Wind analysis

✉ Yan Han
hanyanxj@mail.ustc.edu.cn

[1] School of Earth and Space Sciences, University of Science and Technology of China, Hefei 230026, China

[2] Key Laboratory of Atmospheric Composition and Optical Radiation, Chinese Academy of Sciences, Hefei 230031, China

[3] Northwest Institute of Nuclear Technology of China, Xi'an 710024, China

1 Introduction

Wind measurement is very important for the study of global climate change and the improvement of the accuracy of numerical weather prediction, and the stratospheric wind profiles are of great significance for a flyer platform in the middle and upper atmosphere [1, 2]. At present, there are mainly three means to measure troposphere/stratosphere wind, including rawinsonde, wind profiler radar and lidar [3]. Although the rawinsonde, a primary wind measurement instruments, can probe the wind profile up to 34 km altitude, wind measurements of them are not continuous or with low temporal resolution [4–7]. Wind profiler radars (MST/METEOR/MF radars) provide abundant wind measurements of upper atmospheric for climatological studies. They can continuously probe the altitude range of 0.05–20 and 60–100 km, but the altitude range of 20–60 km is in theirs' blind area, and the measurements with low temporal resolution cannot be used for the study on the fine structure of the atmosphere [4, 7–9]. With lidar technology developed in recent decades, it seems that the lidar has the capability to continuously probe the wind covering the height range of 0.05–110 km with high temporal and vertical resolution better than those of radars [1, 2], meanwhile, the accuracy of wind measurement is equivalent to that of radars.

Direct detection lidar, by use of molecular atmospheric backscattering, plays an important role in the tropospheric and stratospheric wind observation. A few of lidar systems have obtained considerably reliable sounding measurements of the tropospheric and stratospheric wind. The Observatory of Haute Provence (OHP) lidar system set up by Chanin et al. in France is based on the molecular scattering and employs double-edge technology [7], which can detect the wind 8–50 km from entire stratosphere down to tropopause with a vertical resolution of 150 m. The first

wind profiles were acquired at the beginning of 1994 [10]. The wind data by lidar were compared with those by rawinsonde, radar, as well as HWM93 climatological model and ECMWF numerical model, and the results showed good agreement. The mobile lidar system (the GLOW, the Goddard Lidar Observatory for Winds) was developed by the Space Center of the National Aeronautics and Space Administration (NASA Goddard) [11, 12]. GLOW can detect wind with the height range of 1.8–35 km. The system had been employed for radial velocity measurement experiments for 50 h of day and night in North Glen, NH in September 2000, and the measurements were compared with those from rawinsonde, and the results are in good agreement. The Rayleigh/Mie/Raman (RMR) Lidar at the ALOMAR Observatory in Northern Norway (69°N, 16°E) has been equipped with special filters to make daytime measurements of the Rayleigh back-scattered lidar signal at 532, 355 and 1064 nm [7, 13–15]. This system was used for probing the Arctic middle atmosphere wind of the height range of 18–80 km. It probed the upper atmospheric wind in January 2009, which measurements were compared with those of sodium lidar and the ECMWF numerical models, and the agreement is perfect, but continuous wind measurements were not reported yet.

In China, direct detection mobile wind lidar for troposphere and stratosphere has been developed by the University of Science and Technology of China (USTC), and acquired wind measurements in 2010. The lidar system is based on the double-edge technique using Fabry–Perot etalon with triple-bandpass as frequency discriminator, covering the height range of 5–40 km and with a 200 m vertical resolution. This system has been continuously probed the wind of troposphere and stratosphere from 5 to 40 km in Xinjiang region (41.77° N, 86.15° E) for a month in 2010 and three months in 2011. The performance of the lidar system has been reported [16–18], but Lidar observations are not analyzed in detail so far by the group. Quite less wind data from other sounding system were reported in China [19]. In this paper, we analyzed 90-day wind data from the lidar system, and described the characteristics and variation of wind covering 8–40 km altitude range. The wind measurements by lidar with high temporal and vertical resolution are helpful for understanding and predicting weather and climate on all time scales.

2 Instrumentation and methodology

2.1 Description of the mobile Rayleigh Doppler

The mobile Rayleigh Doppler lidar system, relying on Rayleigh backscattering due to air molecules, operates with a Q-switched, injection-seeded, frequency-tripled Nd:YAG laser at 355 nm, a 45-cm aperture telescope. The pulse repetition rate is 30 Hz, and the energy per pulse is ~300–400 mJ at 355 nm. The system relies on the double-edge technique, and the heart of the receiver system is a triple-bandpass Fabry–Perot interferometer (FPI), with two edge bandpasses for a two-point sampling of the Rayleigh backscattered laser line, and with one locking bandpasses for monitoring the laser frequency drift and jitter [20]. The Doppler shift due to the wind is determined from the ratio of the transmissions through each edge bandpass. The system consists of four major modules, which are the laser transmitter, the scanning telescope (transceiver), the photoelectric receivers and controlling system [16], as shown in Fig. 1, and the technical parameters are summarized in Table 1.

The principle of double-edge technique applied in Rayleigh Doppler wind lidar has been described in detail by several groups [21–23], and was not reviewed here. In this paper, the horizontal wind retrieval method is reviewed briefly here. The light-of-sight (LOS) velocity can be expressed as a function of the Doppler shift as:

$$v_{\mathrm{LOS}} = \frac{\lambda}{2}\Delta\upsilon_{\mathrm{d}}, \tag{1}$$

where v_{LOS} is the light-of-sight (LOS) velocity, υ_{d} is the Doppler shift, and λ is the wavelength of the laser. The light-of-sight (LOS) velocity can be expressed as a function of the etalon frequency response function as [23]:

$$v_{\mathrm{LOS}} = \frac{R(\upsilon_{\mathrm{d}}) - R(0)}{R(0)\theta_{\upsilon}}, \tag{2}$$

where $R(\upsilon)$ is the etalon frequency response function, defined as the ratio of the output signal of the two edge-channels, $\theta\nu$ is the sensitivity of the double-edge measurement, defined as the fractional change in the signal ratio of Eq. (3) for a unit wind velocity. R (υ) and $\theta\upsilon$ are given by

$$R(\upsilon_{\mathrm{d}}) = \frac{I_1}{I_2} = \frac{I_3T_1(\upsilon_1+\upsilon_{\mathrm{d}}) + I_4h_1(\upsilon_1+\upsilon_{\mathrm{d}})}{I_3T_2(\upsilon_1+\upsilon_{\mathrm{d}}) + I_4h_2(\upsilon_1+\upsilon_{\mathrm{d}})}, \tag{3}$$

$$\theta_{\upsilon} = \frac{2}{\lambda R(\upsilon)}\frac{\mathrm{d}R(\upsilon)}{\mathrm{d}\upsilon}, \tag{4}$$

where I_1 and I_2 are the intensity of the received signal from each etalon including the Mie and Rayleigh backscatters, I_3 and I_4 are the intensity of the Rayleigh and Mie backscatters, respectively, h_1 (υ) and h_2 (υ) are the transmission function of each etalon including transmission and reflection coefficient of the beamsplitters that are different in each path, υ_1 is the outgoing laser center frequency, υ_{d} is the Doppler frequency shift, and $T_{\mathrm{i}}(\upsilon)$ is the convolution of each etalon transmittance function $h_{\mathrm{i}}(\upsilon)$ and the spectral distribution of Rayleigh–Brillouin signal $f_{\mathrm{R\text{-}B}}$ is given by

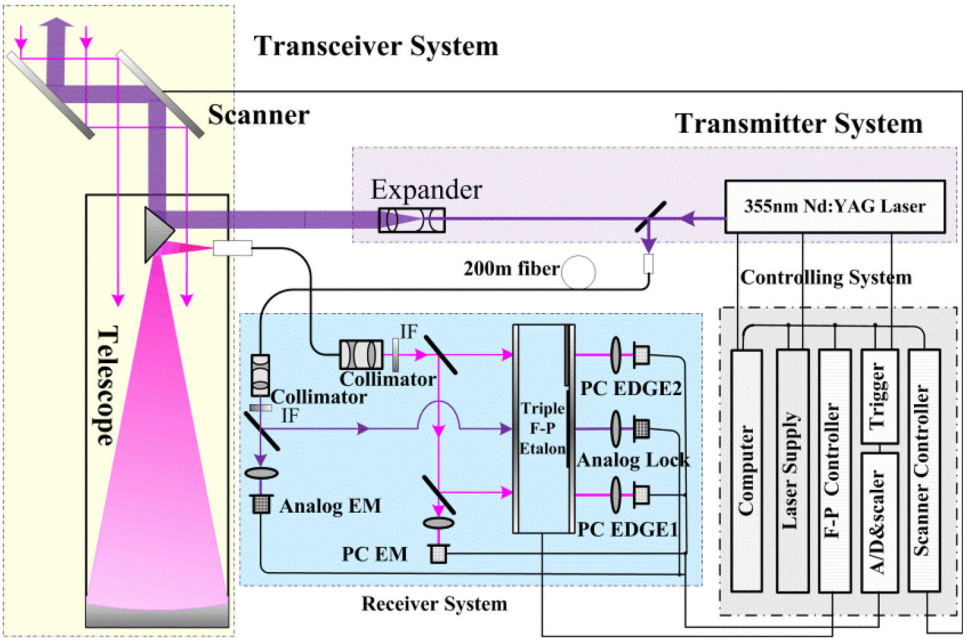

Fig. 1 Schematic diagram of the tropospheric/stratospheric Doppler Lidar system (*IF* interference filters, *PC* photon counting detector, *EM* energy monitor)

Table 1 Technical parameters of the lidar

Parameter	Value
Wavelength (nm)	355
Laser energy/pulse (mJ)	300–400
Laser repetition rate (Hz)	30
Laser 1/e width (MHz)	200
Etalon FSR (GHz)	12
FWHM of edge channels (GHz)	1.7
Etalon peak transmission (%)	60
Edge channel separation (GHz)	5.1
PMT quantum efficiency (%)	20

$$T_{\mathrm{i}}(\upsilon-\upsilon_{\mathrm{i}})=\int_{-\infty}^{\infty} f_{\mathrm{R-B}}(\upsilon-\upsilon_{\mathrm{l}}-\upsilon_{\mathrm{d}})h_{\mathrm{i}}(\upsilon-\upsilon_{\mathrm{i}})\mathrm{d}\upsilon, \tag{5}$$

where $i = 1, 2$ is thυe channel number, υ is the frequency of the laser, υ_{l} is the lock frequency of the laser, i is the center frequency of each etalon, $f_{\mathrm{R\text{-}B}}$ is the spectral distribution of Gauss–Rayleigh signal with $\Delta\upsilon$ spectral width, broadened by atmospheric temperature and pressure, and h_{i} is each etalon transmission function. When parameters of etalon are adapted to Eq. (6), θ_{υ} of Mie backscatters is equal to θ_{υ} of Rayleigh backscatters, and the aerosol signal is not affected on R (υ).

$$\frac{1}{T_{\mathrm{i}}(\upsilon_{\mathrm{l}})}\frac{\mathrm{d}T_i(\upsilon_{\mathrm{l}})}{\mathrm{d}\upsilon}=\frac{1}{h_{\mathrm{i}}(\upsilon_{\mathrm{l}})}\frac{\mathrm{d}h_{\mathrm{i}}(\upsilon_{\mathrm{l}})}{\mathrm{d}\upsilon} \tag{6}$$

Finally, the inversion of Doppler shift υ_{d} with a measured response value $R(\upsilon_{\mathrm{d}})$ is performed by interpolation. Once the Doppler shift is retrieved, the LOS wind velocity is calculated by Eq. (1).

2.2 Retrieval method of the horizontal wind

The lidar system determined the horizontal wind by utilizing the velocity-Azimuth display (VAD) technique [24, 25] and using a four-beam scanning mode. Compared with the three-beam scanning mode, the four-beam scanning mode yields a factor of 2 improvements in the ratio of signal-to-noise, as well as effectively reduces the system-level error [23]. The scanning mode is shown in Fig. 2. In lidar measurements, we sequentially make four line-of-sight (north → south → east → west) wind measurements. The measurements are at a fixed elevation angle of 60°. The line-of-sight winds from the four quadrants are combined to form two orthogonal line-of-sight wind measurements that are used to determine the horizontal components of the vector wind. The horizontal wind velocity and direction is expressed as respectively

$$v_h=\sqrt{v_x^2+v_y^2}, \tag{7}$$

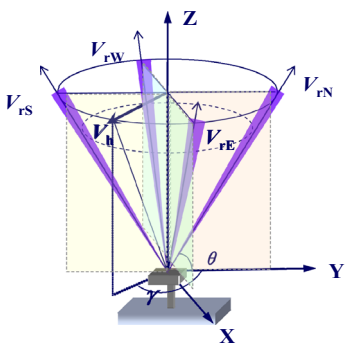

Fig. 2 Schematic diagram of four-beam scanning mode

$$\theta = \arctan\frac{v_y}{v_x} - \frac{\pi}{2}\sin(v_x), \tag{8}$$

where

$$v_x = \frac{V_{rE} - V_{rW}}{2\sin\phi} \quad v_y = \frac{V_{rN} - V_{rS}}{2\sin\phi}, \tag{9}$$

where V_{rE}, V_{rW}, V_{rN} and V_{rS} are the east, west, north and south components of the LOS velocity.

The vertical wind velocity is expressed as:

$$V_z = V_{LOS}\cos\phi \tag{10}$$

where V_{LOS} is the LOS velocity.

3 Lidar validation

The mobile Rayleigh Doppler lidar was successfully developed in 2009, and field wind observations were carried out to evaluate the performance of the system [16]. After improving on the receiver optical structure, temperature control of laser and zero-Doppler correction method, the further comparison of wind measurements by the lidar and the rawinsonde was made every morning 8:00 A.M. from September to October in Xinjiang in 2011. The system conventionally probed the wind starting from 18:00 to 08:00 the next morning. The laser beam was pointed to four-orthogonal at zenith angle of 30°, and the range resolution is 200 m below 20 km altitude and 500 m above 20 km altitude. The measuring time of each line-of-sight (LOS) profile is 7 min, and the horizontal wind velocity and direction can be derived from four LOS profiles every 30 min. The rawinsonde (CASIC, CF-06-A), made in Shanghai, China, used for comparing with the lidar, and its velocity and direction uncertainty are 0.2 m/s and 2° (wind velocity ≥3m/s), respectively, and its balloon can reach 25 km altitude with vertical resolution of 100 m. Wind profile measuring takes rawinsonde about 90 min. The balloon launching location is 12 km away from the lidar. The compared results are shown in Fig. 3, and there are in good agreements between both measurements. Wind measured by Rayleigh Doppler lidar is plotted with error bars. These comparing results show that the lidar system is stable and robust, having the expected good performances.

4 Results and discussion

The mobile Rayleigh Doppler lidar has been applied to routine observations of the 8–40 km altitudes wind in Xinjiang (41.77°N, 86.15°E), China in 2010 and 2011, and continuously probed the wind field from 18:00 to 08:00 next morning in the conditions of clear weather. The 230 valid wind profiles are obtained during 20 days in August and 1510 profiles during 70 days from August to October 2012. The characteristics and variations of wind were analyzed in 1740 profiles.

4.1 Monthly characteristics and variations of the 8–40 km altitudes wind

Figure 4 shows the characteristics and variations of the 5–40 km altitudes wind observed by the lidar in August 2010. In Fig. 4, the wind velocity is within a three-layer structure: westerly jet layer (9–14 km), quasi-zero velocity

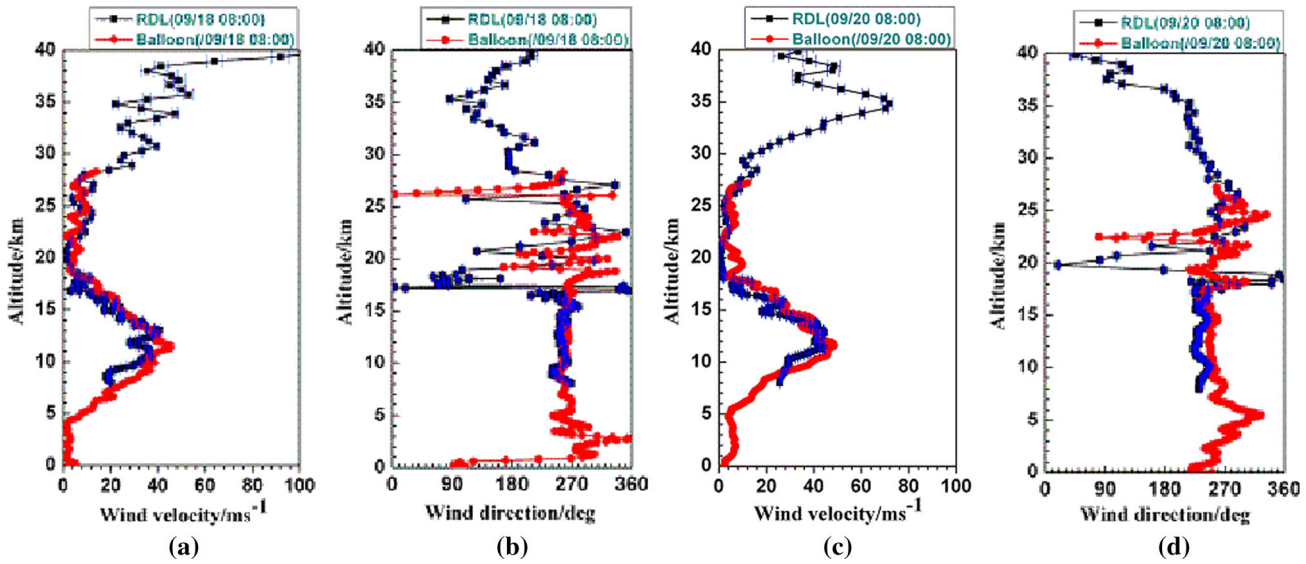

Fig. 3 Profiles of wind speed and direction measured by the Rayleigh Doppler lidar (*line + square symbol*) compared with data measured by radiosonde (*line + rotundity symbol*). In the altitude range, wind velocity and direction *error bars* are plotted

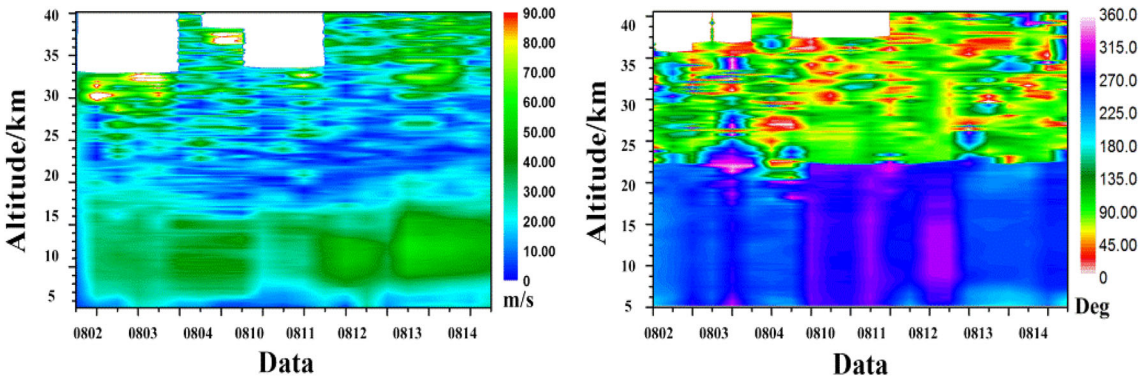

Fig. 4 Time-altitude plots of semi-continuous observations of 5–40 km wind field from 2nd to 15th August, 2010. The data with velocity error larger than 10 m/s are not plotted. The wind direction in the quasi-zero wind layer has no meaning, since the error of velocity measurement is larger than the wind velocity. The minimum velocity error and the minimum direction error in this experiment are estimated to be 1 m/s and 4.2°, respectively

layer (18–22 km) and gale layer (22–40 km), accordingly the wind direction is within a three-layer structure: zonal westerly wind layer (5–18 km) where wind direction is west, zonal wind reverse layer (18–22 km) where wind direction is unstable and easterly wind layer (22–40 km) where wind direction is east. In the westerly jet layer, wind velocity is larger and average wind velocity is 36 m/s and maximum wind velocity is 56 m/s, where wind velocity increases with altitude up to 12 km reaching the maximum, forming a westerly jet center. The height of tropopause is around 11–12 km over Xinjiang from August to October [28], and measured westerly jet center is close to tropopause. In quasi-zero velocity layer, wind velocity decreases with altitude up to 20 km reaching the minimum, where average wind velocity is 11 m/s. In gale layer, the wind velocity increases with altitude again.

Figure 5 shows the characteristics and variations of the 8–40 km altitudes wind in September 2011. In Fig. 5, in early September, the wind velocity is within a three-layer structure: westerly jet layer (9–14 km), quasi-zero velocity layer (18–22 km) and gale layer (22–40 km), accordingly the wind direction is within a three-layer structure: zonal westerly wind layer (5–18 km) where wind direction is west, zonal wind reverse layer (18–22 km) where wind direction is unstable and easterly wind layer (22–40 km) where wind direction is east. In the westerly jet layer, wind velocity is larger and average wind velocity is 34 m/s and maximum wind velocity is 52 m/s, where wind velocity increases with altitude up to 12 km reaching the maximum, forming a westerly jet center. The height of tropopause is around 11–12 km over Xinjiang from August to October [28], and measured westerly jet center is close to tropopause. In quasi-zero velocity layer, wind velocity decreases with altitude up to 20 km reaching the minimum, where average wind velocity is 12 m/s. In gale layer, the wind velocity increases with altitude again. But in late September, above 22 km altitudes range wind direction changes from east to west, and zonal westerly wind layer becomes gradually obscure.

Figure 6 shows the characteristics and variations of 8–40 km wind in October 2011.

In Fig. 6, wind velocity is still within a three-layer structure: westerly jet layer (9–14 km), quasi-zero velocity layer (18–22 km) and gale layer (22–40 km). But throughout 8–40 km altitude range, dominant wind direction is west, and zonal wind reverse layer gradually disappears. In the westerly jet layer, wind velocity is becoming much less than September's, and the average wind velocity is only 23 m/s and maximum wind velocity is only 32 m/s.

Xinjiang (41.77°N, 86.15°E) lies in mid-latitude, over which from 8 to 18 km altitude range, the atmosphere circulation is influenced by tropical high pressure and the rotation of the earth,and is prevailing westerly perennially whether in summer or in winter. The westerly velocity still increases with altitude up to the tropopause (around at 12 km altitude) reaching the maximum, forming a strong westerly center. Its location is relatively stable near tropopause, owing to considerably stable location and intensity of Hadley circulation [26]. In summer, as abnormal heating of lower level atmosphere of the Qinghai–Tibet Plateau and powerful high-pressure of south Asia of upper troposphere cooperating, the strongest westerly location over China moves northwards and westwards to the south of Xinjiang and the west of Inner Mongolia, and corresponds to the westerly jet location of the upper troposphere from 9 to 14 km altitude range [27]. The westerly jet velocity is greatest in August and early September in Xinjiang region, and maximum wind velocity reaches 50 m/s or so. In autumn, the strongest westerly location of upper atmosphere over China moves between the Yellow River and Huaihe River, so the westerly jet velocity over north–west region of China remarkably decreases [27], which leads to the westerly jet velocity considerably decrease over Xinjiang in October, and mean velocity is only

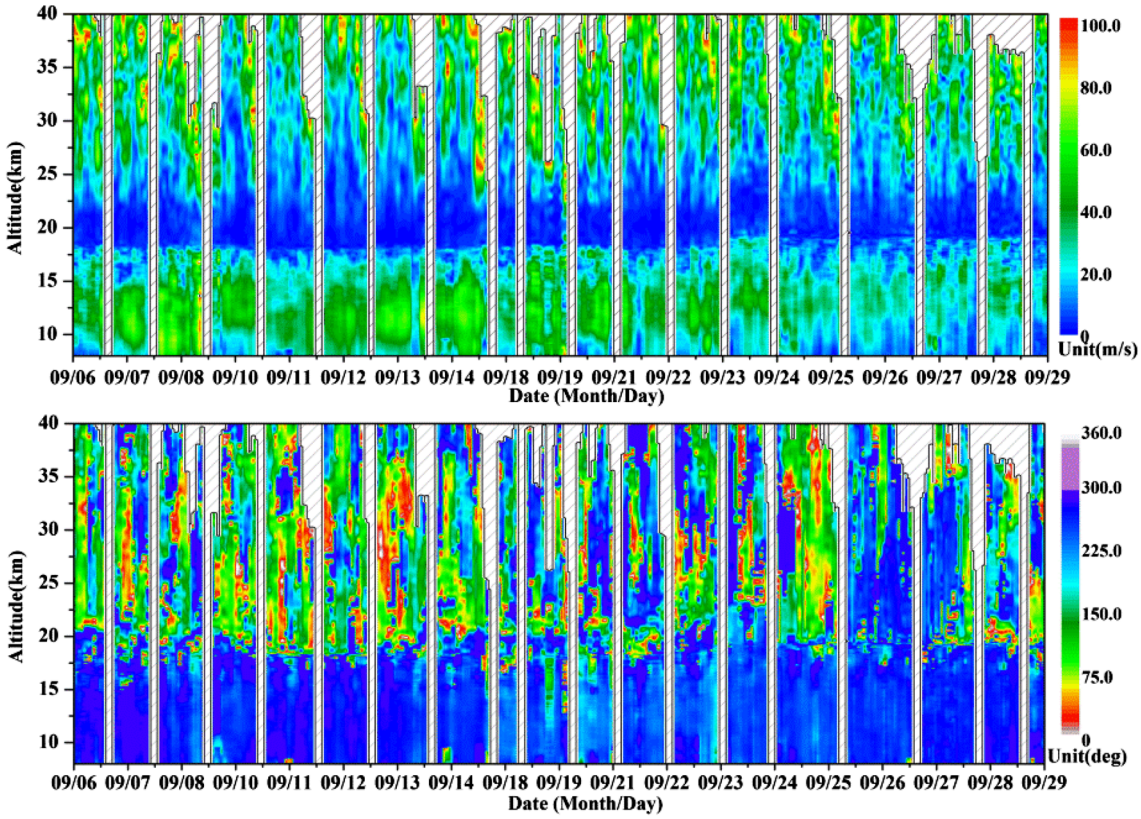

Fig. 5 Time-altitude plots of semi-continuous observations of 8–40 km wind field from 6th to 29th September, 2011. The data with velocity error larger than 10 m/s are not plotted. The wind direction in the quasi-zero wind layer has no meaning, since the error of velocity measurement is larger than the wind velocity. The minimum velocity error and the minimum direction error in this experiment are estimated to be 0.86 m/s and 3.6°, respectively

23 m/s. In summer, because the stratosphere of the entire northern hemisphere is surrounded by high pressure which center lies in polar, the stratosphere prevails stable easterly and the wind direction conversion altitude of stratosphere is 19 km, and wind direction of the stratosphere is east over Xinjiang. In autumn, the lower stratosphere north of 35° N prevails westerly winds under the polar low circulation controlling, and in September and October, the wind direction of the lower stratosphere by lidar measuring of Xinjiang is west. In October, the conversion layer of the stratosphere north of 40° N cannot be found under the polar low circulation controlling, and the conversion layer by lidar measuring of the stratosphere of Xinjiang cannot be found in October. In conclusion, the results of wind measurements by lidar are consistent with seasonal characteristics of the upper wind field in mid-latitude region.

4.2 The characteristics of average wind profile in a month

The average wind profiles in August, September and October have been calculated, and results are shown in Fig. 7. Both in the westerly jet layer and in quasi-zero velocity layer, wind velocity of August is largest, and wind velocity of October is smallest. In gale layer, wind velocity of three months is strong. In zonal westerly wind layer (8–18 km), the wind direction of August and September is west, and wind direction of October is southwest. In zonal wind reverse layer (18–22 km), wind direction rapidly varies from west to east in August, and it varies from west to southwest in September, and it varies from west southeast wind in October. In gale layer (22–40 km), wind direction is southeast wind in August, and it is southwest wind in September and in October.

The occurrence frequency of the east, south, west and north components of wind for a month was calculated and the results are shown in Fig. 8. In zonal westerly wind layer (8–18 km), wind direction is west in August and September, and it is southwest in October. In zonal wind reverse layer (18–22 km), wind direction changes west into east in August. The occurrence frequency of east, west, south and north wind is equivalent in September. In October, the occurrence frequency of west, south wind is slightly larger. In 22–40 km altitude range, wind direction is east in August. In September, the occurrence frequency of east, west, south and north wind is roughly equivalent. In

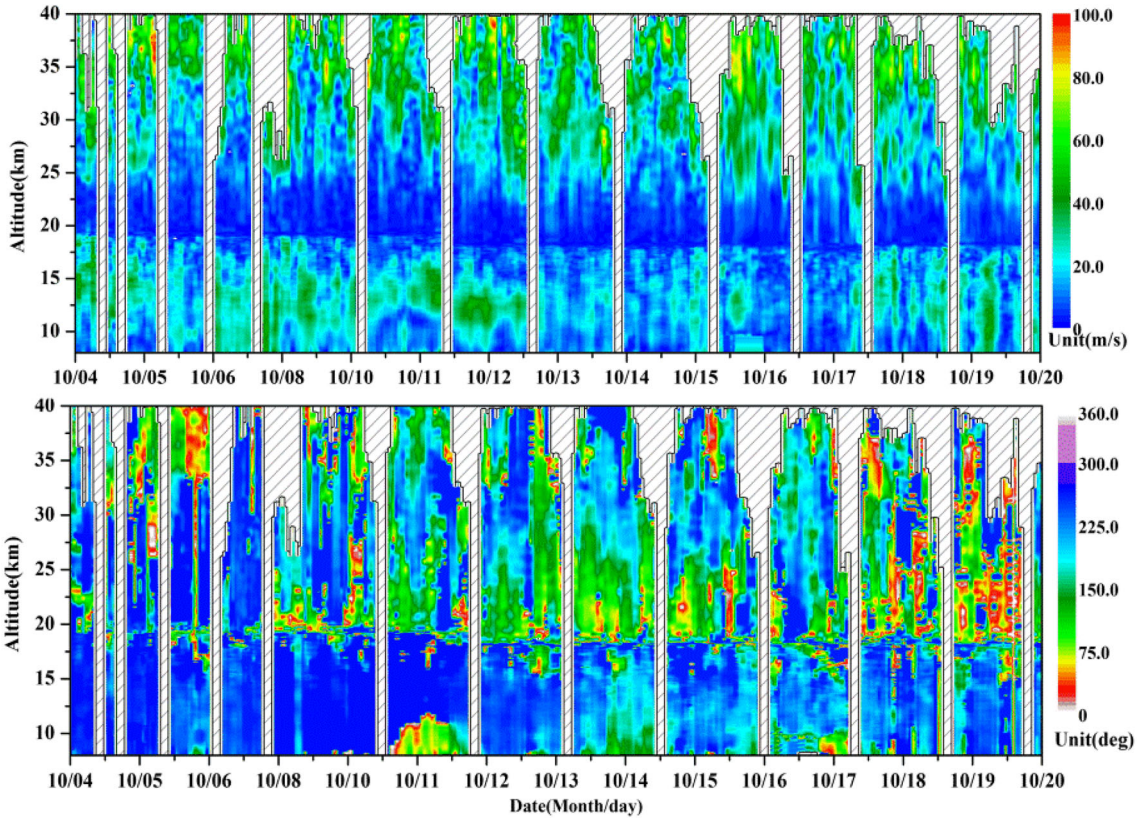

Fig. 6 Time-altitude plots of semi-continuous observations of 8–40 km wind field from 4th to 20th October, 2011. The data with velocity error larger than 10 m/s are not plotted. The wind direction in the quasi-zero wind layer has no meaning, since the error of velocity measurement is larger than the wind velocity. The minimum velocity error and the minimum direction error in this experiment are estimated to be 0.93 m/s and 4°, respectively

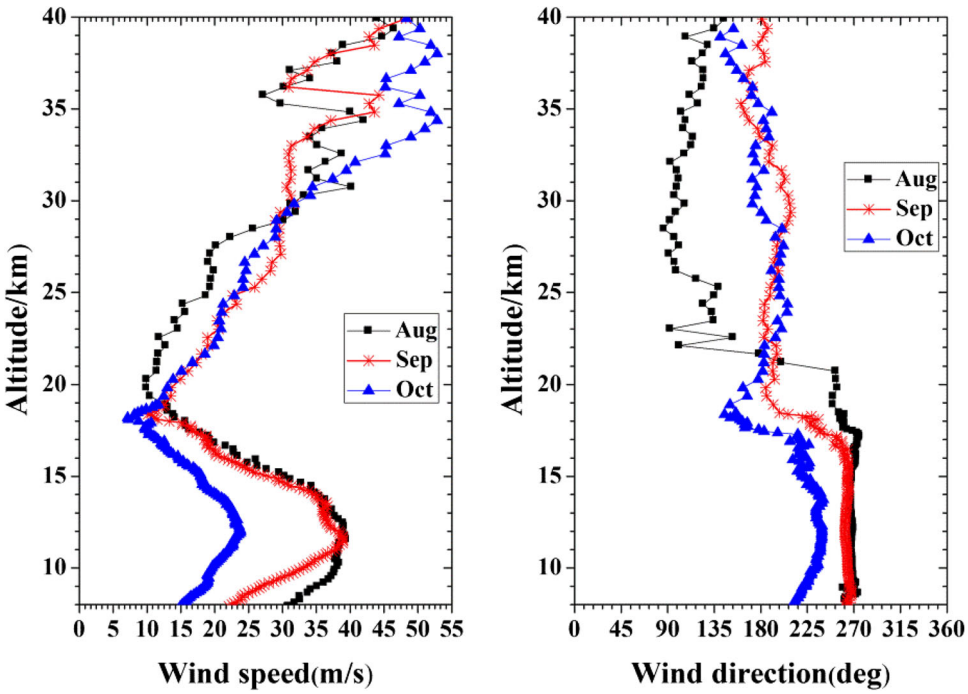

Fig. 7 Average profiles of wind speed and direction measured by the Rayleigh Doppler lidar, average profiles of wind speed and direction in August (*line + square symbol*), average profiles of wind speed and direction in September (*line + star symbol*), average profiles of wind speed and direction in October (*line + triangle symbol*)

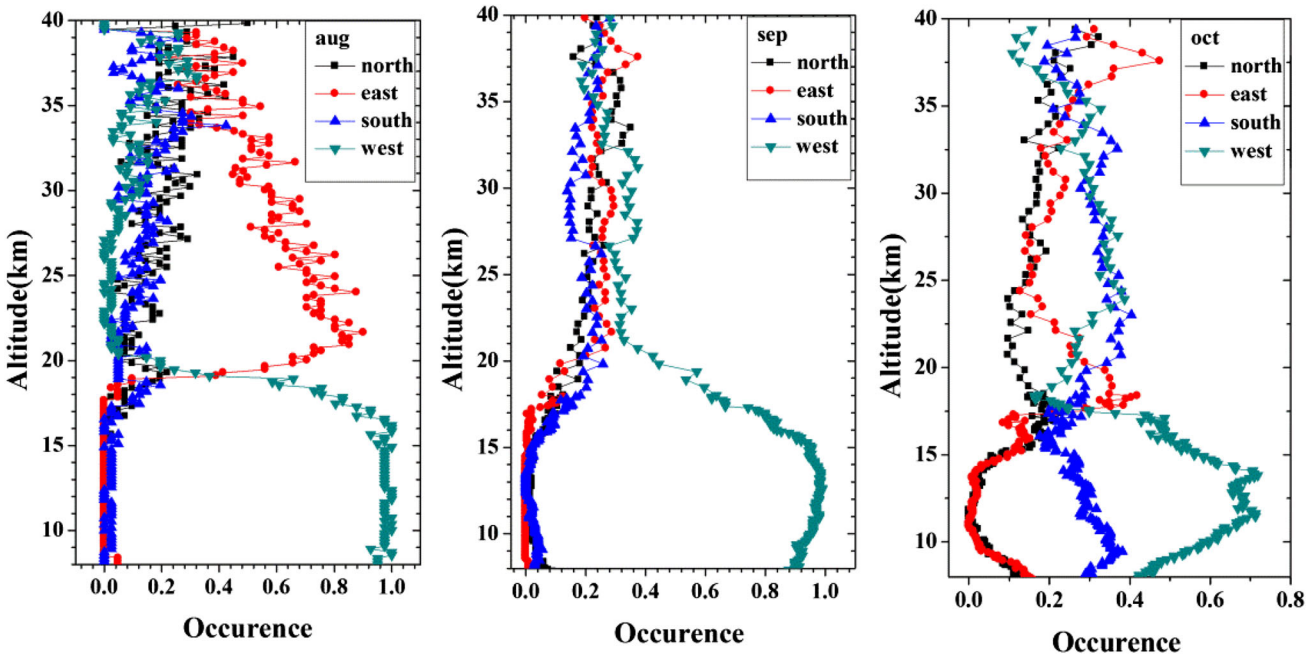

Fig. 8 Occurrence frequency of the east, south, west and north components of wind for a month was calculated, north wind (*line + square symbol*), east wind (*line + rotundity symbol*), south wind (*line + triangle symbol*), and west wind (*line + anti-triangle* symbol)

October, the occurrence frequency of west, south wind is slightly larger.

5 Conclusion

The mobile Rayleigh Doppler lidar based on a Fabry–Perot etalon is successfully developed for 8–40 km wind measurement. Wind observations show the characteristics and variations of the 8–40 km altitudes wind. The wind velocity is within a three-layer structure: westerly jet layer (9–14 km), Quasi-zero velocity layer (18–22 km) and gale layer (22–40 km). In the westerly jet layer, wind velocity is larger, where wind velocity increases with altitude up to 12 km reaching the maximum, forming a westerly jet center. In the westerly jet layer, wind velocity is highest in August and in early September, and decreases in mid-September, and remarkably decreases in October. In Quasi-zero velocity layer, wind velocity decreases with altitude up to 20 km reaching the minimum. Quasi-zero velocity layer is clear in August, and becomes gradually obscure, and gradually disappears in October. In gale layer, the wind velocity increases with altitude again. In August and in September, the wind direction is within a three-layer structure: zonal westerly wind layer (5–18 km) where wind direction is west, zonal wind reverse layer (18–22 km) where wind direction is unstable and easterly wind layer (22–40 km) where wind direction is east. In mid-September, zonal wind reverse layer (18–22 km) becomes gradually obscure, and in easterly wind layer (22–40 km) wind direction changes from east to west. In October, zonal wind reverse layer (18–22 km) becomes disappear, and in easterly wind layer (22–40 km) wind direction changes from east to west, and wind direction is west throughout altitudes of 8–40 km. The results of wind measurements by lidar are consistent with the characteristics of the wind field (8–40 km) in mid-latitude region.

Wind observations by lidar are a realistic offset to the rawinsondes wind, and help us research the atmospheric dynamics. For future research, we will upgrade the lidar for 20–70 km wind observation, and reset a telescope pointing at the zenith of 90° for vertical wind observation, temperature measurement and gravity wave monitoring.

Acknowledgments Jun Guan and Jie Liu are gratefully acknowledged for providing the radiosonde wind measurements in the experiment.

References

1. Salonen, K., Haase, G., Eresmaa, R., Hohtia, H., Järvinena, H.: Towards the operational use of Doppler radar radial winds in HIRLAM. Atmos. Res. **10**, 190 (2011)
2. Baker, W.E., Atlas, R., Cardinali, C., Clement, A., Emmitt, G.D., Gentry, B.M., Michael Hardesty, R., Källén, E., Kavaya, M.J., Langland, R., Ma, Z.Z., Masutani, M., McCarty, W., Bradley Pierce, R., Pu, Z., Riishojgaard, L. P., Ryan, J., Tucker, S., Weissmann, M., Yoe, J.G.: Lidar measured wind profiles: the missing link in the global observing system. Am. Meteorol. Soc. **10**, 543 (2014)

3. Gao, F., Berganta, K., Filipčiča, A., Forte, B., Hua, D.-X., Song, X.-Q., Stanič, S., Veberič, D., Zavrtanik, M.: Observations of the atmospheric boundary layer across the land–sea transition zone using a scanning Mie lidar. J. Quant. Spectrosc. Radiat. Transf. **112**, 182 (2011)
4. Rufenacht, R., Kampfer, N., Murk, A.: First middle-atmospheric zonal wind profile measurements with a new ground-based microwave Doppler-spectro-radiometer. Atmos. Meas. Tech. Discuss. **5**, 5107 (2012)
5. Wang, G., Sun, D., Du, H., Shu, Z., Tang, L., Hu, D., Xu, W., Dong, J., Dou, X.: Analysis of doppler wind lidar detecting data based on Fabry-Perot Etalon. Chin. J. Lasers **38**, 0314002–1 (2011). **(in Chinese)**
6. Liu, Y., Liu, J., Chen, W.: Eye-safe single-frequency pulsed all-fiber laser for Doppler wind lidar. Chin. Opt. Lett. **9**, 090604 (2011)
7. Claude, S., Anne, G., Albert, H.: Rayleigh-Mie Doppler wind lidar for atmospheric measurements II, Mie scattering effect, theory, and calibration. Appl. Opt. **38**, 2422 (1999)
8. Baumgarten, G.: Twin Doppler Rayleigh/Mie/Raman lidar for wind and temperature measurements in the middle atmosphere up to 80km. Atmos. Meas. Tech. Discuss. **3**, 2779 (2010)
9. Sachin, M., Deshpande, P., Raj, E.: UHF wind profiler observations during a tropical pre-monsoon thunderstorm—A case study. Atmos. Res. **93**, 179 (2009)
10. Souprayen, C., Garnier, A., Hertzog, A., Hauchecorne, A., Porteneuve, J.: Rayleigh-Mie Doppler wind lidar for atmospheric measurements. I. Instrumental setup, validation, and first climatological results. Appl. Opt. **38**, 2410 (1999)
11. Gentry, B.M., Chen, H., Li, X.: Wind measurements with 355-nm molecular Doppler lidar. Opt. Lett. **25**, 1231 (2000)
12. Gentry, B., Chen, H.: Tropospheric wind measurements obtained with the Goddard Lidar Observatory for Winds (GLOW) validation and performance. Proc. of the 21st International Laser Radar Conference, Quebec, p. 1 (2002)
13. Rees, D., Vyssogorets, M., Meredith, N.P., Griffin, E., Chaxel, Y.: The Doppler wind and system of the ALOMAR lidar facility: overview and initial results. Atmos. Terr. Phys. **58**, 1827 (1996)
14. Von, Z.U., Von, C.G., Fiedler, J., Fricke, K.H., Nelke, G., Baumgarten G., David R., Hauchecorne, A., Adolfsen, K.: The ALOMAR Rayleigh/Mie/Raman lidar: objectives, configuration, and performance. Ann. Geophys. **18**, 815 (2000)
15. Hildebrand, J, Baumgarten, G, Fiedler, J, Hoppe, U-P., Kaifler, B., Lübken, F.-J., Williams, B.P.: Combined wind measurements by two different lidar instruments in the Arctic middle atmosphere. Atmos. Meas. Tech. Discuss. **5**, 4123 (2012)
16. Tang, L., Wang, Y., Shu, Z., Dong, J., Wang, G., Xu, W., Hu, D., Dou, T.C.X., Sun, D., Cha, H.: Analysis of detectors and transmission curve correction of mobile rayleigh Doppler wind lidar. Chin. Phys. Lett. **27**, 114207 (2010)
17. Dou, X., Han, Y., Sun, D., Xia, H., Shu, Z., Zhao, R., Shangguan, M., Guo, J.: Mobile Rayleigh Doppler lidar for wind and temperature measurements in the stratosphere and lower mesosphere. Opt. Express **22**, A1203 (2014)
18. Han, Y., Sun, D., Dou, X., Xia, H., Shu, Z., Zhao, R., Shangguan, M., Gao, Y.: Frequency drift control for wind measurements by UV Rayleigh Doppler lidar. J. Quant. Spectrosc. Radiat. Transf. **10**, 1016 (2014)
19. Ren, G., Zhang, A., Wang, Y., Guo, J.: Climatology of upper wind speeds over China. Geogr. Res. **28**, 1583 (2009)
20. Zhang, F., Dou, X., Sun, D., Shu, Z., Xia, H., Gao, Y., Hu, D., Shangguan, M.: Analysis on error of laser frequency locking for fiber optical receiver in direct detection wind lidar based on Fabry-Perot interferometer and improvements. Opt. Eng. **53**, 124102–1 (2014)
21. Flesia, C., Korb, C.L.: Theory of the double-edge molecular technique for Doppler lidar wind measurement. Appl. Opt. **38**, 432 (1999)
22. Sun, D., Li, Y.: Doppler lidar for both high and low altitude wind detection. Infrared Laser Eng. **37**, 237 (2008). **(in Chinese)**
23. Laurence Korb, C., Gentry, B.M., Li, S.X., Flesia, C.: Theory of the double-edge technique for Doppler lidar wind measurement. Appl. Opt. **37**, 3097 (1998)
24. Gentry, B.M., Laurence Korb, C.: Edge technique for high-accuracy Doppler velocimetry. Appl. Opt. **33**, 5770 (1994)
25. Huffaker, R.M.: Laser Doppler detection systems for gas velocity measurement. Appl. Opt. **9**, 1026 (1970)
26. Ma, r., Liao, H.: Chin.: The characteristics of winds at height of 20–80km in the Chinese area. J. Sp. Sci. **19**, 334 (1999)
27. ZHang, A., Ren, G., Guo, J., Wang, Y.: Change trend analyses on upper-air wind speed over China in past 30 years. Plateau Meteorol. **28**, 680 (2009)
28. Xu, X., Gao, P., Zhang, X.: Structure and variation of the tropopause over China with COSMIC radio occultation bending angles. Chin. J. Geophys. **56**, 2531 (2013)